In Figs. 3 and 4, the union upper and lower bounds on the average SERs of the DF relay and the AF relay with STBC-CIOD are plotted versus the SNR in quasi-static uncorrelated Rayleigh fading channels, which are compared with the SER results obtained by Monte Carlo simulations. From the figures, the tightness of the derived union upper bound for the true SER with the various modulation types is obviously observed, whereas the curves for the lower bound are relatively loose, but still maintaining their asymptotic diversity orders. From the numerical results, it is apparent that our theoretically derived results show good agreement with the simulation results.

V. Conclusion and Future Work

In this paper, considering the dual-hop relay transmission in DF and AF protocols with STBC-CIOD, the union upper and lower bounds on the average SER and the achievable asymptotic diversity order have been analyzed. The theoretically derived union bounds are in good agreement with the simulation results and provide a good basis for the extension to more general relay topologies incorporating STBC-CIOD. Our performance evaluations provided in this paper can be extended to more general relay systems employing more than two antennas, additionally with/without a direct link between the source and the destination.

References

[1] D. Soldani and S. Dixit, "Wireless relays for broadcast access," *IEEE Commun. Mag.*, vol. 46, no. 3, pp. 58–66, Mar. 2008.
[2] Q. Zhang, J. Jia, and J. Zhang, "Cooperative relay to improve diversity in cognitive radio networks," *IEEE Commun. Mag.*, vol. 47, no. 2, pp. 111–117, Feb. 2009.
[3] G. Kramer, M. Gastpar, and P. Gupta, "Cooperative strategies and capacity theorems for relay networks," *IEEE Trans. Inf. Theory*, vol. 51, no. 9, pp. 3037–3063, Sep. 2005.
[4] A. Abdaoui, S. S. Ikki, and M. H. Ahmed, "Performance analysis of MIMO cooperative relaying system based on Alamouti STBC and amplify-and-forward schemes," in *Proc. IEEE Int. Conf. Commun.*, Cape Town, South Africa, May 2010, pp. 1–6.
[5] M. O. Hasna and M. S. Alouini, "End-to-end performance of transmission systems with relays over Rayleigh-fading channels," *IEEE Trans. Wireless Commun.*, vol. 2, no. 6, pp. 1126–1131, Nov. 2003.
[6] M. O. Hasna and M. S. Alouini, "A performance study of dual-hop transmissions with fixed gain relays," *IEEE Trans. Wireless Commun.*, vol. 3, no. 6, pp. 1963–1968, Nov. 2004.
[7] I. H. Lee and D. W. Kim, "Decouple-and-forward relaying for dual-hop Alamouti transmissions," *IEEE Commun. Lett.*, vol. 12, no. 2, pp. 97–99, Feb. 2008.
[8] I. H. Lee and D. W. Kim, "End-to-end BER analysis for dual-hop OSTBC transmissions over Rayleigh fading channels," *IEEE Trans. Commun.*, vol. 56, no. 3, pp. 347–351, Mar. 2008.
[9] J. B. Kim and D. W. Kim, "Performance of dual-hop amplify-and-forward beamforming and its equivalent systems in Rayleigh fading channels," *IEEE Trans. Commun.*, vol. 58, no. 3, pp. 729–732, Mar. 2010.
[10] J. Yindi and B. Hassibi, "Distributed space–time coding in wireless relay networks," *IEEE Trans. Wireless Commun.*, vol. 5, no. 12, pp. 3524–3536, Dec. 2006.
[11] C. Hucher, G. R. B. Othman, and J. C. Belfiore, "AF and DF protocols based on Alamouti ST code," in *Proc. IEEE Int. Symp. Inf. Theory*, Nice, France, Jun. 2007, pp. 1526–1530.
[12] M. Z. A. Khan, "Single-symbol and double-symbol decodable STBCs for MIMO fading channels," Ph.D. dissertation, Indian Inst. Sci., Bangalore, India, Jul. 2003.
[13] M. Z. A. Khan and B. S. Rajan, "Single-symbol maximum likelihood decodable linear STBCs," *IEEE Trans. Inf. Theory*, vol. 52, no. 5, pp. 2062–2091, May 2006.
[14] H. Lee, J. G. Andrews, R. W. Heath, Jr., and E. J. Powers, "The performance of space–time block codes from coordinate interleaved orthogonal designs over nakagami-m fading channels," *IEEE Trans. Commun.*, vol. 57, no. 3, pp. 653–664, Mar. 2009.
[15] S. Alamouti, "A simple transmit diversity technique for wireless communications," *IEEE J. Sel. Areas Commun.*, vol. 16, no. 8, pp. 1451–1458, Oct. 1998.
[16] S. Chennakeshu and J. B. Anderson, "Error rates for Rayleigh fading multichannel reception of MPSK signals," *IEEE Trans. Commun.*, vol. 43, no. 234, pp. 338–346, Feb.–Apr. 1995.
[17] I. S. Gradshteyn and I. M. Ryzhik, *Table of Integrals, Series and Products*, 7th ed. San Diego, CA: Academic, 2007.

Joint Decoding of LDPC Code and Phase Factors for OFDM Systems With PTS PAPR Reduction

Li Li and Daiming Qu

***Abstract*—In this paper, we investigate a low-density parity-check (LDPC)-coded orthogonal frequency-division multiplexing (OFDM) system with a peak-to-average power ratio (PAPR) reduction using the partial transmit sequence (PTS), which does not transmit PTS side information about the phase factors. We view the PTS processing as a stage of coding and call the resulted code of LDPC coding and PTS processing a concatenated LDPC-PTS code. Then, we derive the parity-check matrix of the concatenated LDPC-PTS code. With the parity-check matrix, the LDPC code and phase factors can be jointly decoded using belief propagation algorithms. Neither transmission of PTS side information (phase factors) nor phase factor estimation before decoding is required by the proposed scheme. Simulation results show that the proposed joint decoding provides nearly perfect phase factor recovery and LDPC decoding for a small number of PTS partitions.**

***Index Terms*—Low-density parity check (LDPC), orthogonal frequency-division multiplexing (OFDM), partial transmit sequence (PTS), peak-to-average power ratio (PAPR), Tanner graph.**

I. Introduction

It is well known that orthogonal frequency-division multiplexing (OFDM) has been adopted in various wireless communication standards. However, it suffers from a high peak-to-average power ratio (PAPR). Among the techniques [1] that have been proposed to reduce the PAPR, the partial transmit sequence (PTS) [2], [3] has attracted a lot of attention because it introduces no distortion in the transmitted signal and achieves significant PAPR reduction. However, one of the critical challenges of PTS schemes is that the phase factor information is required to be transmitted to the receiver as side information, which decreases transmission efficiency and increases system complexity.

Recently, some works [4]–[7] have been presented for phase factor recovery with the help of error-correcting codes, which do not require the transmission of phase factor information. In [4], a maximum-likelihood decoder to recover phase factors was derived based on the

Manuscript received May 18, 2012; revised August 11, 2012 and September 26, 2012; accepted September 28, 2012. Date of publication October 3, 2012; date of current version January 14, 2013. This work was supported in part by the National Science Foundation of China under Grant 61271228 and in part by the Fundamental Research Funds for the Central Universities, Huazhong University of Science and Technology, under Grant 2012TS019. The review of this paper was coordinated by Prof. H. H. Nguyen. *(Corresponding author: Daiming Qu)*

The authors are with the Department of Electronics and Information Engineering, Huazhong University of Science and Technology, Wuhan 430074, China (e-mail: lili_unique@hust.edu.cn; qudaiming@mail.hust.edu.cn).

Color versions of one or more of the figures in this paper are available online at http://ieeexplore.ieee.org.

Digital Object Identifier 10.1109/TVT.2012.2222455

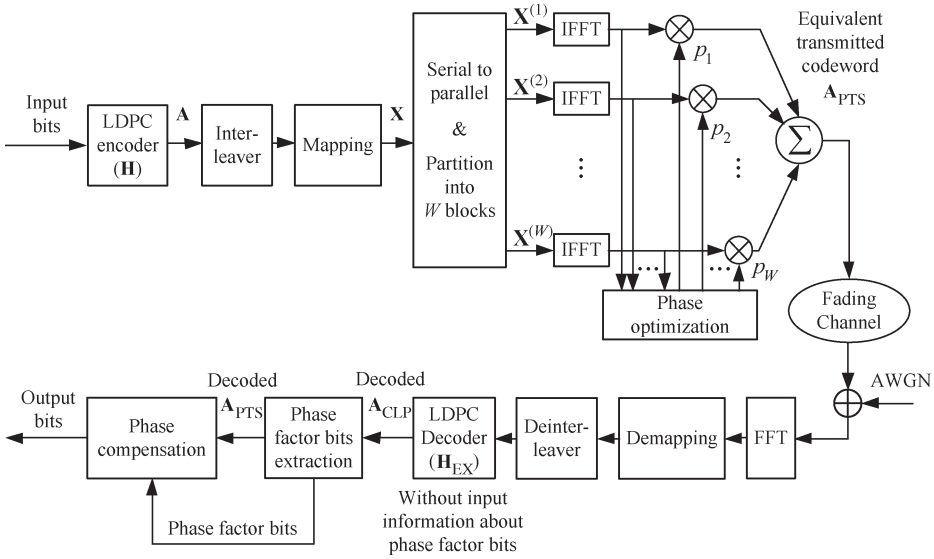

Fig. 1. System diagram of the proposed joint decoding scheme.

fact that the signals generated by the PTS scheme with different phase factors are widely different in Hamming distance. Phase factor estimation methods were proposed in [5] and [6], which exploit the extrinsic outputs of the Turbo/low-density parity-check (LDPC) decoder. In [7], a blind estimation method was proposed, which decodes all possible candidates by the Turbo decoder using one or two iterations to find the most probable candidate. Different from all the aforementioned methods, we propose a scheme that does not have to perform phase factor estimation before decoding.

The novelty of this paper is that we propose joint decoding of the LDPC code and phase factors, which simply uses belief propagation (BP) algorithms [9] and could enable a simple system design. In this paper, we investigate an LDPC-coded OFDM system with the PTS PAPR reduction, which does not transmit PTS side information about the phase factors. We view the PTS processing as a stage of coding and call the resulted code of LDPC coding and PTS processing a concatenated LDPC-PTS code. Then, we derive the parity-check matrix of the concatenated LDPC-PTS code. With the parity-check matrix, the LDPC code and phase factors can be jointly decoded using BP algorithms.

Notation: Bold fonts will be used to denote vectors and matrices; $[\cdot]^T$ will represent transpose of a matrix.

II. Joint Decoding of Low-Density Parity Check Code and Partial Transmit Sequence Phase Factors

A. Concatenated LDPC-PTS Code

In the LDPC-coded OFDM system shown in Fig. 1, an LDPC [8] codeword is mapped onto OFDM subcarriers with phase-shift keying (PSK) modulation/quadrature-amplitude modulation (QAM). The LDPC codeword, which is denoted by row vector $\mathbf{A}$, is mapped onto one OFDM data block of N_c subcarriers after a random interleaver. Denote the data block by vector $\mathbf{X} = [X(1), \ldots, X(N_c)]$, where $X(k)$ represents the PSK/QAM symbol on the kth subcarrier. With the PTS PAPR reduction, $\mathbf{X}$ is partitioned into W blocks, i.e., $\mathbf{X}^{(1)}, \ldots, \mathbf{X}^{(W)}$, where $\mathbf{X}^{(w)} = [X^{(w)}(1), \ldots, X^{(w)}(N_c)]$, for $w = 1, 2, \ldots, W$. The partition satisfies that $X^{(w)}(k) = 0$ or $X(k)$ for $k = 1, 2, \ldots, N_c$ and $w = 1, 2, \ldots, W$, and $\sum_{w=1}^{W} \mathbf{X}^{(w)} = \mathbf{X}$. Then, the candidate data block of PTS, which is denoted by $\mathbf{X}_{\mathrm{PTS}}$, can be obtained by independently rotating $\mathbf{X}^{(w)}$ with the phase factor p_w $(w = 1, 2, \ldots, W)$, i.e.,

$$\mathbf{X}_{\mathrm{PTS}} = \sum_{w=1}^{W} p_w \mathbf{X}^{(w)}. \tag{1}$$

The phase factors that minimize the PAPR of the OFDM data block are employed in the PTS processing.

In this paper, we assume that $p_w \in \{1, -1\}$ for all w. We also assume that the PSK modulation/QAM scheme employed in the system satisfies the following: multiplying the PSK/QAM symbols by a phase factor of -1 flips several bits of the symbols and does not change the other bits, and the indexes of bits that are flipped when the symbols are multiplied by -1 are common to all symbols and known to the receiver. Obviously, the widely adopted PSK modulation/QAM with Gray mapping satisfies this assumption. As an example, there are two bits standing for the sign of the I- and Q-phase components, respectively, among the four bits of a Gray mapping 16-QAM symbol. In the case of multiplying Gray mapping 16-QAM symbols by a phase factor of -1, these two sign bits are always flipped, and the other two bits are never changed. Let $\mathbf{A}_w$ $(w = 1, 2, \ldots, W)$ denote the row vector of the bits that are flipped when p_w is turned from 1 to -1, and let $\mathbf{A}_0$ denote the row vector of all other bits that are never affected by the PTS processing. This way, the original LDPC codeword $\mathbf{A}$ is divided into $W + 1$ vectors, i.e., $\mathbf{A}_0, \mathbf{A}_1, \ldots, \mathbf{A}_W$. Denote the length of vector $\mathbf{A}_w$ by N_w for $w = 0, 1, \ldots, W$.

The corresponding vectors after the PTS processing are denoted by $(\mathbf{A}_{\mathrm{PTS}})_0, (\mathbf{A}_{\mathrm{PTS}})_1, \ldots, (\mathbf{A}_{\mathrm{PTS}})_W$, respectively. Apparently, $(\mathbf{A}_{\mathrm{PTS}})_0 = \mathbf{A}_0$. Due to the PTS processing and the aforementioned assumptions, we have

$$(\mathbf{A}_{\mathrm{PTS}})_w = \mathbf{A}_w \oplus [\underbrace{b_w, \ldots, b_w}_{N_w}], \quad \text{for } w = 1, 2, \ldots, W \tag{2}$$

where $\oplus$ represents modulo-2 addition, and b_w represents the phase factor bit of the wth block, i.e.,

$$b_w = \begin{cases} 0, & p_w = 1, \\ 1, & p_w = -1, \end{cases} \quad \text{for } w = 1, 2, \ldots, W. \tag{3}$$

We call $\mathbf{A}_{\mathrm{PTS}}$ as the equivalent transmitted codeword in this paper.

In this paper, the concatenated LDPC-PTS codeword is defined as the codeword consisting of the equivalent transmitted codeword and phase factor bits, although the phase factor bits are not transmitted by the system.

Definition 1: The *concatenated LDPC-PTS code* for the previously described OFDM system is a block code with the following codeword, which is represented by a vector of bits:

$$\mathbf{A}_{\mathrm{CLP}} = [\mathbf{A}_0, (\mathbf{A}_{\mathrm{CLP}})_1, \ldots, (\mathbf{A}_{\mathrm{CLP}})_W] \tag{4}$$

where $(\mathbf{A}_{\mathrm{CLP}})_w = [(\mathbf{A}_{\mathrm{PTS}})_w, b_w]$, for $w = 1,\ 2, \ldots, W$.

Apparently, the equivalent transmitted codeword $\mathbf{A}_{\mathrm{PTS}}$ is a punctured version of the concatenated LDPC-PTS codeword $\mathbf{A}_{\mathrm{CLP}}$. In the rest of this section, we define the extended Tanner graph for the OFDM system and discuss its relationship with the concatenated LDPC-PTS code.

B. Extended Tanner Graph

An LDPC code is a linear block code defined by a sparse parity-check matrix or its equivalent bipartite graph, which is also called a Tanner graph. Let $\mathbf{H}$ of dimension $M \times N$ and $(\mathbf{V}, \mathbf{C}, \mathbf{E})$ denote the parity-check matrix and Tanner graph of the LDPC code in the previously described system, respectively, where $\mathbf{V} = \{v_1, v_2, \ldots, v_N\}$ is the variable-node set, $\mathbf{C} = \{c_1, c_2, \ldots, c_M\}$ is the check-node set, $\mathbf{E}$ is the set of edges, and $\mathbf{E} \subseteq \mathbf{V} \times \mathbf{C}$.

We divide the variable-node set into $W+1$ disjoint subsets according to the partition of PTS, i.e., $\mathbf{V} = \mathbf{V}_0 \cup \mathbf{V}_1 \cup \cdots \cup \mathbf{V}_W$, where $\mathbf{V}_w (w = 0, 1, \ldots, W)$ corresponds to the bit vector $\mathbf{A}_w$. Next, we define the extended Tanner graph as follows.

Definition 2: The *extended Tanner graph* $(\mathbf{V}_{\mathrm{EX}}, \mathbf{C}, \mathbf{E}_{\mathrm{EX}})$ for the previously described OFDM system is extended from $(\mathbf{V}, \mathbf{C}, \mathbf{E})$ with the following rule: the extended variable-node set $\mathbf{V}_{\mathrm{EX}}$ consists of subsets $\mathbf{V}_0, (\mathbf{V}_{\mathrm{EX}})_1, \ldots, (\mathbf{V}_{\mathrm{EX}})_W$, where $(\mathbf{V}_{\mathrm{EX}})_w$ is the extension of the subset $\mathbf{V}_w$ by including phase factor node b_w, i.e., $(\mathbf{V}_{\mathrm{EX}})_w = \mathbf{V}_w \cup \{b_w\}$, for $w = 1, 2, \ldots, W$. In addition, the extended edge set $\mathbf{E}_{\mathrm{EX}}$ consists of $\mathbf{E}$ and new edges that are connected to phase factor nodes $b_1, b_2, \ldots, b_W$. The new edges are generated with the following rule: For any check node $c \in \mathbf{C}$ and phase factor node b_w, $w = 1, 2, \ldots, W$, an edge is added between c and phase factor node b_w if the total number of edges connecting c to all variable nodes in $\mathbf{V}_w$ is odd. (Without sacrificing clarity, we abuse the notation b_w for the phase factor node and phase factor bit in this paper.)

An example of the extended Tanner graph is presented in Fig. 2, in which phase factor nodes b_1 and b_2 are inserted into the Tanner graph for variable-node subsets $\mathbf{V}_1$ and $\mathbf{V}_2$, respectively. In addition, four edges (between c_3 and b_1, c_5 and b_1, c_4 and b_2, and c_5 and b_2) are added in the extended Tanner graph so that the total number of edges connecting each check node to all variable nodes in $(\mathbf{V}_{\mathrm{EX}})_w$ $(w = 1, 2)$ is even.

As a Tanner graph defines a parity-check matrix, we can obtain the extended parity-check matrix $\mathbf{H}_{\mathrm{EX}}$ of dimension $M \times (N + W)$ from $(\mathbf{V}_{\mathrm{EX}}, \mathbf{C}, \mathbf{E}_{\mathrm{EX}})$. $\mathbf{H}_{\mathrm{EX}}$ consists of $W+1$ submatrices as

$$\mathbf{H}_{\mathrm{EX}} = [\mathbf{H}_0, (\mathbf{H}_{\mathrm{EX}})_1, \ldots, (\mathbf{H}_{\mathrm{EX}})_W] \tag{5}$$

where $(\mathbf{H}_{\mathrm{EX}})_w$ $(1 \le w \le W)$ is the submatrix of $\mathbf{H}_{\mathrm{EX}}$, whose columns correspond to the extended variable-node subset $(\mathbf{V}_{\mathrm{EX}})_w$, and $\mathbf{H}_0$ is the submatrix corresponding to $\mathbf{V}_0$.

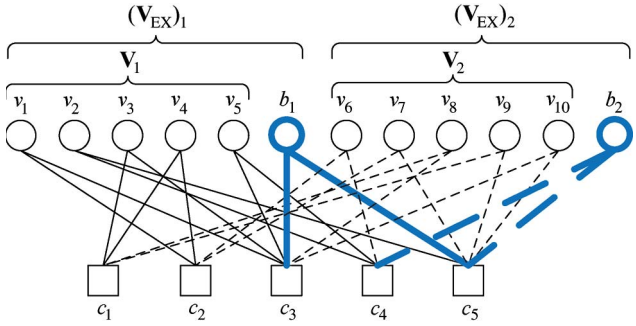

Fig. 2. Example of the extended Tanner graph.

C. Parity-Check Matrix and Decoding of the Concatenated LDPC-PTS Code

Theorem 1: The concatenated LDPC-PTS code for the previously defined OFDM system is a linear block code with parity-check matrix $\mathbf{H}_{\mathrm{EX}}$ and Tanner graph $(\mathbf{V}_{\mathrm{EX}}, \mathbf{C}, \mathbf{E}_{\mathrm{EX}})$.

Proof: It can be written over GF(2) for $1 \le w \le W$

$$\begin{aligned}
&(\mathbf{H}_{\mathrm{EX}})_w\,[(\mathbf{A}_{\mathrm{CLP}})_w]^T \\
&\quad = (\mathbf{H}_{\mathrm{EX}})_w\,[(\mathbf{A}_{\mathrm{PTS}})_w, b_w]^T \\
&\quad = (\mathbf{H}_{\mathrm{EX}})_w\,[a_w(1) \oplus b_w, \ldots, a_w(N_w) \oplus b_w, b_w]^T \\
&\quad = (\mathbf{H}_{\mathrm{EX}})_w\,[a_w(1), \ldots, a_w(N_w), 0]^T \\
&\qquad + (\mathbf{H}_{\mathrm{EX}})_w[\underbrace{b_w, \ldots, b_w}_{N_w}, b_w]^T \\
&\quad = \mathbf{H}_w[\mathbf{A}_w]^T + (\mathbf{H}_{\mathrm{EX}})_w[b_w, \ldots, b_w, b_w]^T
\end{aligned} \tag{6}$$

where $\mathbf{H}_w$ is the submatrix of $\mathbf{H}$, whose columns correspond to the variable-node subset $\mathbf{V}_w$, and $a_w(k)$ is the kth element of $\mathbf{A}_w$.

Since the total number of edges connecting each check node to all variable nodes in $(\mathbf{V}_{\mathrm{EX}})_w$ is even, each row of the associated submatrix $(\mathbf{H}_{\mathrm{EX}})_w$ has even Hamming weight (even number of 1s) $(1 \le w \le W)$. Therefore

$$(\mathbf{H}_{\mathrm{EX}})_w[\underbrace{b_w, \ldots, b_w}_{N_w}, b_w]^T = \mathbf{0}, \quad \text{for } 1 \le w \le W. \tag{7}$$

Then, we have

$$(\mathbf{H}_{\mathrm{EX}})_w\,[(\mathbf{A}_{\mathrm{CLP}})_w]^T = \mathbf{H}_w[\mathbf{A}_w]^T, \qquad \text{for } 1 \le w \le W. \tag{8}$$

Finally, we have

$$\begin{aligned}
\mathbf{H}_{\mathrm{EX}}[\mathbf{A}_{\mathrm{CLP}}]^T &= \mathbf{H}_0[\mathbf{A}_0]^T + \sum_{w=1}^{W} (\mathbf{H}_{\mathrm{EX}})_w\,[(\mathbf{A}_{\mathrm{CLP}})_w]^T \\
&= \sum_{w=0}^{W} \mathbf{H}_w[\mathbf{A}_w]^T = \mathbf{H}[\mathbf{A}]^T = \mathbf{0}.
\end{aligned} \tag{9}$$

Therefore, the concatenated LDPC-PTS codeword $\mathbf{A}_{\mathrm{CLP}}$ is a valid codeword of the linear block code with parity-check matrix $\mathbf{H}_{\mathrm{EX}}$ and Tanner graph $(\mathbf{V}_{\mathrm{EX}}, \mathbf{C}, \mathbf{E}_{\mathrm{EX}})$. ■

Fig. 1 also shows the receiver diagram of the proposed joint decoding scheme. Since $\mathbf{A}_{\mathrm{PTS}}$ is the puncture version of the concatenated LDPC-PTS codeword $\mathbf{A}_{\mathrm{CLP}}$, $\mathbf{A}_{\mathrm{CLP}}$ can be decoded with $\mathbf{H}_{\mathrm{EX}}$ and the received $\mathbf{A}_{\mathrm{PTS}}$. Note that the decoded $\mathbf{A}_{\mathrm{CLP}}$ consists of the decoded $\mathbf{A}_{\mathrm{PTS}}$ and phase factor bits. Assuming correct decoding,

TABLE I
PROPORTION OF NONZERO ELEMENTS AND DEGREES OF PHASE NODES IN THE PARITY-CHECK MATRIX $\mathbf{H}$ AND $\mathbf{H}_{\mathrm{EX}}$ WITH DIFFERENT W, A CODE RATE OF 1/2, AND QPSK MODULATION

	Proportion of Non-zero Elements	Degrees of $b_1, \cdots, b_W$
$\mathbf{H}$	0.0070	NA
$\mathbf{H}_{\mathrm{EX}}, W = 2$	0.0080	250, 257
$\mathbf{H}_{\mathrm{EX}}, W = 4$	0.0090	228, 266, 268, 265
$\mathbf{H}_{\mathrm{EX}}, W = 6$	0.0098	243, 244, 221, 250, 228, 255
$\mathbf{H}_{\mathrm{EX}}, W = 8$	0.0104	215, 211, 210, 224, 218, 218, 203, 232

phase factor bits are extracted, and then, the original LDPC codeword $\mathbf{A}$ can be found by phase compensation as the following:

$$\mathbf{A}_w = \begin{cases} (\mathbf{A}_{\mathrm{PTS}})_w \oplus [\underbrace{b_w, \ldots, b_w}_{N_w}], & w = 1, 2, \ldots, W \\ \mathbf{A}_0, & w = 0. \end{cases} \tag{10}$$

The complexity of the proposed joint decoding is higher, but not very significant, compared with that of decoding of the original LDPC code, since the dimension of the parity-check matrix of the concatenated LDPC-PTS code ($\mathbf{H}_{\mathrm{EX}}$) is only greater than that of the original LDPC code ($\mathbf{H}$) for W columns, and $W \ll N$.

III. SIMULATION RESULTS

Here, we demonstrate the performance of the proposed joint decoding of LDPC codeword and phase factor bits by computer simulation. The OFDM system employs LDPC codes of length 1008, a random interleaver, QPSK modulation or 16-QAM, and a cyclic prefix of length 1/4 of the symbol duration. There are $N_c = 504$ and $N_c = 252$ subcarriers for QPSK modulation and 16-QAM, respectively. For the LDPC codes of all rates, we obtain good degree distribution pairs with maximum variable-node degree $d_{v_{\max}} = 10$ by the density evolution technique [10] and construct the parity-check matrices $\mathbf{H}$ by the progressive edge-growth algorithm [12] with the optimized variable-node degree distribution. The PTS scheme employs the pseudorandom partition method described in [1], and each partition consists of N_c/W subcarriers for all simulations, except for the case with 16-QAM and $W = 8$. For the case with 16-QAM and $W = 8$, the first partition has 35 subcarriers, and each of the other partitions has 31 subcarriers. Without sacrificing the PAPR performance [2], the first partition among the W partitions has a fixed phase factor of 1. In all the following simulations, the phase factor bits are not transmitted by the transmitter. The receiver employs a log-likelihood ratio BP decoder.

Table I shows the proportion of nonzero elements in the parity-check matrix $\mathbf{H}$ and $\mathbf{H}_{\mathrm{EX}}$ for different W, with the code rate of 1/2 and QPSK modulation. This verifies that both $\mathbf{H}_{\mathrm{EX}}$ and $\mathbf{H}$ are sparse, and the complexity of the proposed joint decoding is higher, but not very significant, compared with that of decoding of the original LDPC code.

It is noted that four cycles are difficult to be avoided when extending the Tanner graph, as described in Section II. However, it is well known that not all short cycles are equally harmful. Apparently, all four cycles generated by extending the Tanner graph involve the phase nodes, the degrees of which are high in general. As an example, the degrees of phase nodes are also presented in Table I. Since high-degree variable nodes could get more information from their check nodes, they tend to correct their values quickly. This is noted in [11]. In addition, high-degree variable nodes are less likely to lead to low-weight codes [12], stopping sets, and trapping sets. Therefore, the four cycles involving high-degree phase nodes are not as harmful to error-correcting performance as those formed by lower degree nodes. Based on the foregoing analysis, we anticipate that the performance of the proposed joint decoding scheme is only insignificantly degraded from the original LDPC code when W is small. In addition, the performance degradation will be larger when W is larger because more phase factor bits have to be recovered and because of the larger number of four cycles. In the following, we will verify these through simulations of the error performance of the proposed joint decoding scheme.

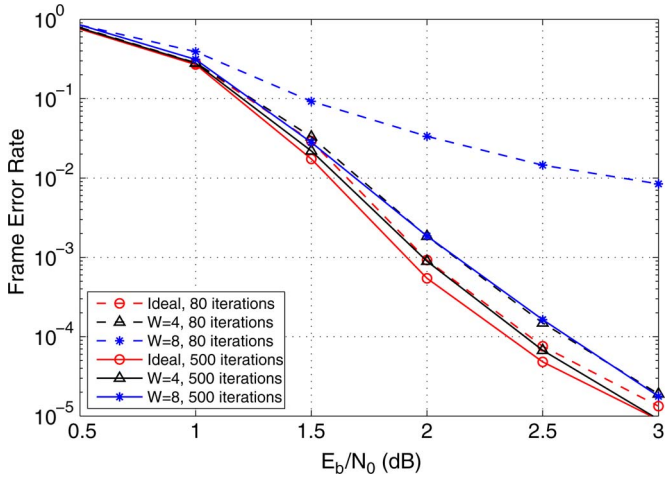

Fig. 3. FER performance of the proposed joint decoding with different numbers of decoding iterations, different W, a code rate of 1/2, and QPSK modulation over an AWGN channel.

Fig. 3 presents the frame-error-rate (FER) performance of the proposed joint decoding with different numbers of decoding iterations, different W, a code rate of 1/2, and QPSK modulation over an additive white Gaussian noise (AWGN) channel. FER performance of decoding with ideal phase factor information is also presented for comparison. It is worth noting that the error rate performance of decoding of $\mathbf{A}_{\mathrm{CLP}}$ with check matrix $\mathbf{H}_{\mathrm{EX}}$ and ideal phase factor information $b_w (1 \le w \le W$; the error rate performance of the ideal case) is equivalent to that of decoding of the original LDPC code $\mathbf{A}$ with check matrix $\mathbf{H}$, whereas the PTS phase rotation is assumed to be already compensated before decoding. Moreover, the LDPC codes employed in the simulation are among the codes with the best error-correcting performance known to date. It is observed from Fig. 3 that the FER performance of the proposed joint decoding gets closer to that of the ideal case with the increasing of decoding iterations. In addition, the BP decoder requires more iterations to converge for larger W. For example, at an FER of 10^{-3}, when $W = 4$, it would take 80 iterations, and when $W = 8$, it would take 500 iterations to obtain a performance that is 0.2 dB degraded from the ideal case. In the following, we employ a maximum of 500 iterations for all the simulations.

The bit-error-rate (BER) and FER curves of the proposed joint decoding with different W, different code rates, and QPSK modulation over an AWGN channel are plotted in Fig. 4. It is observed that the proposed joint decoding achieves FER performance that is very close to that of the ideal case for small W. For example, compared with the ideal case, the performance degradation at an FER of 10^{-3} is less than 0.2 dB for $W = 2$, 4, and 6 at the code rate of 1/2. For the code rate of 3/4, the FER performance loss is less than 0.2 dB when W is equal to or lower than 4. The slight FER performance gap shows that the proposed joint decoding provides nearly perfect phase factor recovery and LDPC decoding for small W. It is also observed from Fig. 4 that the BER performance gap between the case of the proposed joint decoding and the ideal case is larger than its corresponding FER performance gap due to the error propagation

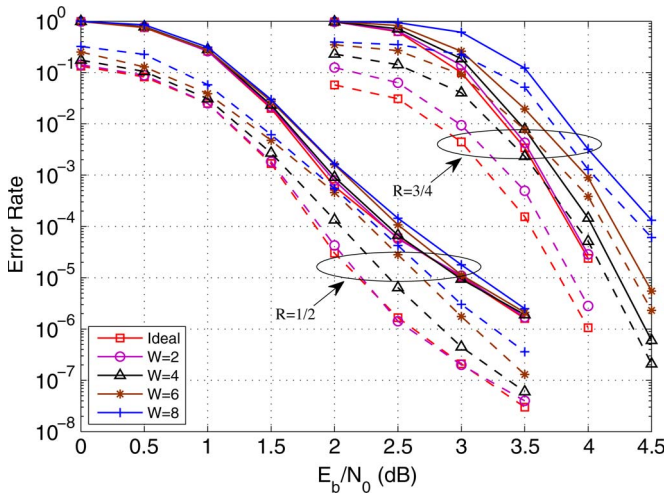

Fig. 4. (Dashed lines) BER and (solid lines) FER performance of the proposed joint decoding with different W, different code rates, and QPSK modulation over an AWGN channel.

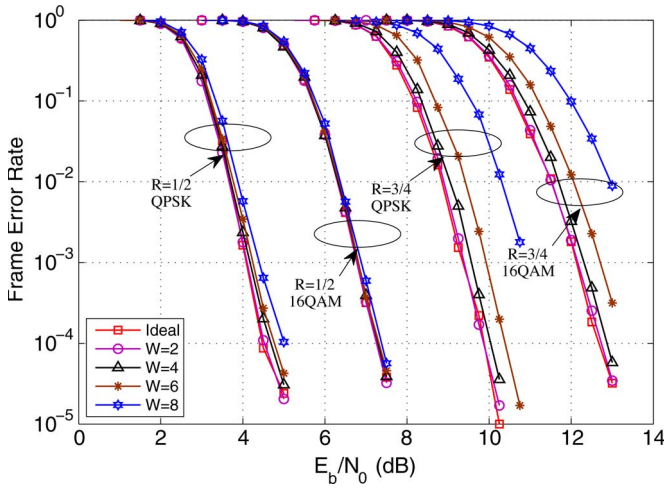

Fig. 5. FER performance of the proposed joint decoding with different W, different code rates, QPSK modulation, and 16-QAM over an uncorrelated Rayleigh fading channel.

that occurs with fail-decoded phase bits. Nevertheless, the FER is a measure of performance that is more important than the BER for communication systems with an automatic repeat request (ARQ) mechanism.

Fig. 5 presents FER performance of the proposed joint decoding with different W, different code rates, QPSK modulation, and 16-QAM over an uncorrelated Rayleigh fading channel. It is observed that the proposed joint decoding provides nearly perfect phase factor recovery and LDPC decoding for small W under an uncorrelated Rayleigh fading channel as well.

Fig. 6 presents the complementary cumulative distribution functions (CCDFs) of the PAPR for the original OFDM signal and those with the PTS processing, with QPSK modulation and 16-QAM. The OFDM signals are four times oversampled in the time domain to approximate the PAPR of continuous-time OFDM signals in the simulation. It is observed from Fig. 6 that the PTS processing offers about 0.8-, 2.2-, 3.1-, and 3.7-dB PAPR reductions for QPSK modulation at CCDF $= 10^{-4}$ when $W = 2$, 4, 6, and 8, respectively. It is worth emphasizing that the proposed joint decoding scheme is a receiver-side scheme. In another words, the transmitter of the proposed scheme is the same as that of the usual LDPC-coded OFDM system with the

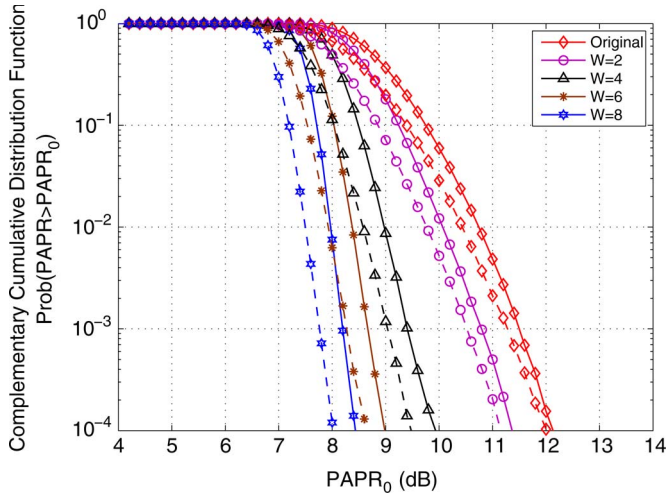

Fig. 6. PAPR performance of the OFDM system with different W. (Solid lines) QPSK modulation. (Dashed lines) 16-QAM. There are 504 and 252 subcarriers for QPSK modulation and 16-QAM, respectively.

PTS PAPR reduction, which is shown in Fig. 1. Therefore, the PAPR performance of the simulated system is exactly the same as that of the well-known PTS technique. These results show that the proposed scheme can provide a significant PAPR reduction, as well as nearly perfect phase factor recovery and LDPC decoding, with small W.

IV. Conclusion and Future Works

In this paper, we have derived the parity-check matrix of the concatenated LDPC-PTS code. With the parity-check matrix, the LDPC codeword and phase factor bits can be jointly decoded using BP algorithms. Simulation results showed that the proposed joint decoding provides nearly perfect phase factor recovery and LDPC decoding for a small partition number W. Most importantly, the proposed joint decoding could simplify the design of OFDM systems with the PTS PAPR reduction in the following two aspects: 1) It does not require the transmission of phase factor bits (i.e., the PTS side information), and 2) it does not require phase factor estimation before LDPC decoding as in existing works [4]–[7]. Therefore, the PTS technique, together with the proposed joint decoding scheme, could serve as an attractive solution for the PAPR reduction of OFDM systems.

Since there is always a requirement for a further PAPR reduction, it remains an important topic for future works to improve the proposed scheme to support a larger partition number W, with enhanced convergence speed of decoding and no significant degradation of the error-correcting performance. Possible solutions may include a joint design of the LDPC code and PTS scheme at the transmitter to obtain concatenated LDPC-PTS codes of better performance, as well as an improved decoding algorithm to overcome the effect of four cycles of the concatenated LDPC-PTS code.

References

[1] T. Jiang and Y. Wu, "An overview: Peak-to-average power ratio reduction techniques for OFDM signals," *IEEE Trans. Broadcast.*, vol. 54, no. 2, pp. 257–268, Jun. 2008.

[2] S. H. Muller and J. B. Huber, "OFDM with reduced peak-to-average power ratio by optimum combination of partial transmit sequences," *IEE Electron. Lett.*, vol. 33, no. 5, pp. 368–369, Feb. 1997.

[3] L. J. Cimini and N. R. Sollenberger, "Peak-to-average power ratio reduction of an OFDM signal using partial transmit sequences," *IEEE Commun. Lett.*, vol. 4, no. 3, pp. 86–88, Mar. 2000.

[4] A. D. S. Jayalath and C. Tellambura, "SLM and PTS peak-power reduction of OFDM signals without side information," *IEEE Trans. Wireless Commun.*, vol. 4, no. 5, pp. 2006–2013, Sep. 2005.
[5] O. Muta and Y. Akaiwa, "Weighting factor estimation method for peak power reduction based on adaptive flipping of parity bits in Turbo-coded OFDM systems," *IEEE Trans. Veh. Technol.*, vol. 57, no. 6, pp. 3551–3562, Nov. 2008.
[6] O. Muta and Y. Akaiwa, "Peak power reduction method based on structure of parity-check matrix for LDPC coded OFDM transmission," in *Proc. IEEE Veh. Technol. Conf.*, Apr. 2007, pp. 2841–2845.
[7] Y. C. Tsai and Y. L. Ueng, "Multiple-candidate separation for PTS-based OFDM systems by Turbo decoding," in *Proc. IEEE Veh. Technol. Conf.*, May 2010, pp. 1–5.
[8] R. G. Gallager, "Low density parity check codes," *IRE Trans. Inf. Theory*, vol. IT-8, no. 1, pp. 21–28, Jan. 1962.
[9] T. Richardson and R. Urbanke, "The capacity of low-density parity check codes under message-passing decoding," *IEEE Trans. Inf. Theory*, vol. 47, no. 2, pp. 599–618, Feb. 2001.
[10] T. J. Richardson, A. Shokrollahi, and R. Urbanke, "Design of capacity approaching irregular low-density parity-check codes," *IEEE Trans. Inf. Theory*, vol. 47, no. 2, pp. 619–637, Feb. 2001.
[11] M. Luby, M. Mitzenmacher, A. Shokrollahi, and D. Spielman, "Improved low-density parity-check codes using irregular graphs," *IEEE Trans. Inf. Theory*, vol. 47, no. 2, pp. 585–598, Feb. 2001.
[12] X. Y. Hu, E. Eleftheriou, and D. M. Arnold, "Regular and irregular progressive edge-growth Tanner graphs," *IEEE Trans. Inf. Theory*, vol. 51, no. 1, pp. 386–398, Jan. 2005.

Performance Analysis of Hybrid Wireless Networks Under Bursty and Correlated Traffic

Yulei Wu, Geyong Min, and Laurence T. Yang

***Abstract*—Wireless local area networks (WLANs) have risen in popularity for in-car networking systems that are designed to make driving safer. Wireless mesh networks (WMNs) are widely deployed to expand the coverage of high-speed WLANs and to support last-mile connectivity for mobile users anytime and anywhere at low cost. Many recent measurement studies have shown that the traffic arrival process in wireless networks exhibits the bursty and correlated nature. A new analytical model is developed in this paper as a cost-effective performance tool to investigate the quality-of-service (QoS) of the WMN that interconnects multiple WLANs in the presence of bursty and correlated traffic. After validating its accuracy via extensive simulation experiments, the analytical model is then used to investigate the performance of the hybrid wireless networks.**

***Index Terms*—Analytical modeling, bursty and correlated traffic, integrated wireless networks, Internet, wireless mesh networks (WMNs).**

Manuscript received March 30, 2012; revised July 15, 2012; accepted August 26, 2012. Date of publication September 19, 2012; date of current version January 14, 2013. This work was supported in part by the National Program on Key Basic Research Project (973 Program) under Grant 2012CB315803 and in part by the "Strategic Priority Research Program" of the Chinese Academy of Sciences under Grant XDA01020304. The review of this paper was coordinated by Prof. A. Boukerche.

Y. Wu is with the China Science and Technology Network, Computer Network Information Center, Chinese Academy of Sciences, Beijing 100190, China (e-mail: wuyulei@cstnet.cn).

G. Min is with the Department of Computing, School of Computing, Informatics and Media, University of Bradford, Bradford BD7 1DP, U.K. (e-mail: g.min@brad.ac.uk).

L. T. Yang is with the School of Computer Science and Technology, Huazhong University of Science and Technology, Wuhan 430074, China, and also with the Department of Computer Science, St. Francis Xavier University, Antigonish, NS B2G 2W5, Canada (e-mail: ltyang@stfx.ca).

Digital Object Identifier 10.1109/TVT.2012.2219890

I. Introduction

The ever-growing number of vehicles on roads creates numerous traffic-related problems for our society. Wireless local area networks (WLANs) have risen in popularity as European automakers have made progress on in-car networking systems that are designed to enhance driving safety. Wireless mesh networks (WMNs) are widely used to expand the coverage of high-speed WLANs and are developed to offer rapid development and easy reconfiguration of wireless broadband communications, as well as to support last-mile connectivity for mobile users anytime and anywhere at low cost [1], [10], [18]. Mesh routers (MRs) facilitated with the gateway functionality can be connected to the Internet and are often called gateways.

Performance studies on WLANs and WMNs have been widely reported in the literature [2], [3], [11], [12], [14]. For example, Bianchi [2] developed an original analytical model to calculate the throughput of WLANs subject to the IEEE 802.11 distributed coordination function (DCF) medium-access control (MAC) protocol. This model can be applied to both packet transmission schemes, i.e., the basic DCF mechanism and the request-to-send/clear-to-send mechanism. Liu and Lin [12] investigated the burst transmission and the acknowledgement aggregation in the IEEE 802.11e WLANs under unsaturated traffic loads and error-prone channel conditions. Mahani *et al.* [14] presented an analytical model to investigate the performance of a MAC scheme in WMNs. Their work considered the hidden terminals and the coexisting of control and data traffic at different frequency channels. In [11], a test bed to investigate a quality-of-service (QoS) scheme based on rate-adaptive admission control methods for multimedia multicast communications in WMNs is employed. Furthermore, many state-of-the-art algorithms, protocols, and performance studies of wireless networks have been reported in [3]. For example, a set of admission control and resource reservation schemes was presented for QoS provisioning in wireless networks, and the evolution in the design of the IEEE 802.11 DCF MAC protocol was illustrated.

The analytical models for the hybrid WLANs and WMNs, particularly with respect to the packet delay, loss probability, and throughput analysis, are rarely found in the current literature. Recently, Niyato and Hossain [17] have presented a bandwidth management and admission control framework for the integrated WLANs and multihop infrastructure mesh networks. However, the QoS prediction of such hybrid wireless networks was not carried out. To fill in this gap, an analytical model was proposed in [16] to investigate the delay and throughput in the integrated WLANs and Internet-access mesh networks. However, the model was based on the assumption that the packets generated by the wireless user terminals (UTs) follow the nonbursty Poisson process.

Multimedia applications over mobile wireless networks are becoming more and more popular [13]. Many recent measurement studies have revealed that the traffic arrival process in wireless networks exhibits bursty and correlated nature, which has a considerable impact on the network performance. In this paper, a new analytical model is developed as a cost-effective performance tool to investigate the QoS metrics, including the packet delay, loss probability, and throughput of the WMNs that interconnect multiple WLANs in the presence of bursty and correlated traffic. The WMN acts as the multihop backhaul network with the gateway being connected to the Internet [16]. Each MR is connected to one access point (AP) that manages a specific WLAN containing multiple UTs. Each network entity (i.e., UT, AP, and MR) is equipped with one finite-capacity buffer. Packets in the WMN are transmitted in a multihop manner toward or from the gateway. The developed model adopts the Markov-modulated Poisson process (MMPP) to capture the bursty and correlated nature of the